

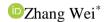
Technobius Physics

https://technobiusphysics.kz/

e-ISSN 3007-0147

Article

Thickness- and gate-tunable ferromagnetism in low-dimensional Fe₃GeTe₂ nanoflakes



School of Materials Science and Engineering, Taizhou University, Taizhou, China *Correspondence: weiz17863@gmail.com

Abstract. This study investigates thickness- and gate-dependent magnetism in low-dimensional van der Waals ferromagnet Fe₃GeTe₂ nanoflakes. The objective was to quantify how critical magnetic parameters evolve when approaching the two-dimensional limit and under electrostatic carrier modulation. High-quality single crystals were grown by self-flux, and flakes with thicknesses between 7.5 and 26 nm were isolated, encapsulated with hexagonal boron nitride, and fabricated into Hall-bar devices. Magnetotransport, polar magneto-optical Kerr effect, and SQUID magnetometry were employed to probe Curie temperature, coercive field, anisotropy, anomalous Hall conductivity, and interlayer exchange. The results reveal a systematic reduction of Curie temperature from 206 K at 26 nm to 156 K at 7.5 nm, consistent with finite-size scaling. Coercive field increased nearly threefold across the same thickness range, accompanied by high anisotropy fields of 4-6 T, indicating enhanced surface-driven perpendicular magnetic anisotropy. Anomalous Hall conductivity rose with thickness and was dominated by intrinsic Berry curvature contributions. Magnetooptical measurements confirmed weakening of interlayer exchange coupling from 0.12 to 0.06 mJ·m⁻² as thickness decreased, marking the crossover toward quasi-two-dimensional behavior. Electrostatic gating of intermediate-thickness flakes shifted the Curie temperature by approximately 5 K per 1013 cm⁻² carrier density and reduced coercivity by about 10%, demonstrating effective electrical control of itinerant ferromagnetism. These findings establish a coherent picture of how thickness and carrier density tune magnetic order in Fe₃GeTe₂ nanoflakes. The results address the central research problem and highlight pathways for exploiting electrically tunable two-dimensional magnets in low-power spintronic applications.

Keywords: ferromagnetism, low-dimensional systems, Fe₃GeTe₂, anomalous Hall effect, perpendicular magnetic anisotropy, electrostatic gating.

1. Introduction

Magnetism in low-dimensional systems has become a central research direction in condensed matter physics. Reducing dimensionality to the nanometer scale alters exchange interactions, enhances thermal fluctuations, and amplifies surface-induced anisotropy [1]. Such effects challenge the classical Mermin-Wagner theorem, which prohibits long-range order in strictly two-dimensional isotropic systems, and create opportunities for stabilizing novel magnetic states in van der Waals (vdW) layered crystals [2]. These advances are of both fundamental importance and practical relevance for energy-efficient spintronic devices. Van der Waals magnets such as CrI₃, Cr₂Ge₂Te₆, and Fe₃GeTe₂ (FGT) have recently emerged as model systems for exploring these effects [3], [4]. Among them, FGT is a metallic ferromagnet with strong perpendicular magnetic anisotropy and itinerant carriers, which makes it a promising candidate for electrical control of magnetism [5]. Despite progress, several challenges remain unresolved. The thickness dependence of the Curie temperature (T_c) and coercive field (H_c) has not been systematically quantified, with different studies reporting scattered values. The contribution of interlayer exchange to stabilizing long-range order near the few-layer limit also remains unclear. Furthermore, while electrostatic gating has been demonstrated as a powerful tuning method in insulating magnets [6], its influence on metallic vdW ferromagnets has been insufficiently explored.

Several recent works have attempted to address these issues. Authors of the paper [7] demonstrated the persistence of ferromagnetism in exfoliated FGT and reported thickness-dependent suppression of T_c , but without a rigorous scaling analysis. Other researchers observed robust perpendicular magnetic anisotropy and anomalous Hall transport in FGT nanoflakes, yet did not systematically study coercivity trends [8]. [9] showed that gating could reversibly control interlayer coupling in CrI_3 bilayers, though such behavior in metallic systems remains to be clarified. [10] proposed a scaling relation to distinguish intrinsic and extrinsic contributions to the anomalous Hall effect, but comprehensive experimental validation in FGT nanostructures is still lacking.

The unresolved problem is the absence of a coherent framework that quantitatively unifies the effects of thickness, anisotropy, interlayer exchange, and gate modulation in metallic vdW magnets. Without such systematic investigation, design of low-dimensional spintronic devices is hindered by uncertainties in tunability and stability.

Hypothesis. We hypothesize that the suppression of interlayer exchange with decreasing thickness reduces T_c , while surface anisotropy enhances coercivity. Furthermore, we propose that electrostatic gating modifies the carrier density at the Fermi level, thereby tuning exchange interactions and enabling electrical control of magnetic order.

The objective of this study is to experimentally establish the thickness and gate dependences of Tc, Hc, anisotropy field, anomalous Hall conductivity, and interlayer exchange in Fe₃GeTe₂ nanoflakes. By combining magnetotransport, magneto-optical, and magnetometry techniques, we aim to construct a consistent picture of low-dimensional ferromagnetism in metallic vdW systems. The novelty lies in unifying finite-size scaling, Berry-curvature-driven transport, and electrostatic tunability within a single experimental framework.

2. Methods

2.1 Crystal growth and exfoliation

Bulk Fe₃GeTe₂ single crystals were synthesized by the self-flux method following established protocols [11], [12]. High-purity Fe (99.99%), Ge (99.999%), and Te (99.999%) powders were mixed in a molar ratio of 3:1:10, sealed in evacuated quartz ampoules, and heated to 950 °C for 12 h. The melt was slow-cooled to 600 °C at 2 °C/h, after which excess flux was removed by centrifugation. Crystals were stored in an argon-filled glovebox ($O_2/H_2O < 0.1$ ppm).

Thin flakes with thickness between 6–30 nm were obtained by mechanical exfoliation using adhesive tape and transferred onto SiO_2/Si substrates (285 nm oxide). Hexagonal boron nitride (hBN, 10–20 nm) was employed as a protective encapsulation layer. Flake thickness was determined by tapping-mode atomic force microscopy (AFM, Bruker Dimension Icon) with ± 0.2 nm precision, cross-validated with optical contrast calibration [13].

2.2 Device fabrication

Hall-bar devices were patterned using electron-beam lithography (Raith eLINE Plus). Contacts were defined by Ar plasma etching followed by Cr/Au (5/60 nm) deposition using an electron-beam evaporator (Kurt J. Lesker PVD75). Gate dielectrics consisted of hBN flakes (15–20 nm), transferred onto FGT using a polypropylene carbonate/poly(dimethylsiloxane) stamp. Top-gate electrodes of Ti/Au (5/50 nm) were deposited in the same chamber. Device geometries were typically $W=2-4~\mu m$ and $L=6-12~\mu m$.

2.3 Magnetotransport measurements

Transport measurements were conducted in a closed-cycle cryostat with a 9T superconducting vector magnet (Quantum Design PPMS). Longitudinal (R_{xx}) and transverse (R_{xy}) resistances were measured using a standard four-probe lock-in technique (Stanford SR830, excitation frequency 17 Hz, current bias 1–10 μ A). The anomalous Hall resistance was isolated by subtracting the linear

ordinary Hall contribution determined at high fields [14]. Carrier densities were tuned by electrostatic gating in the range $-5\text{V} \le V_g \le +5\text{ V}$, corresponding to $|\Delta n| \lesssim 1.2 \times 10^{13} \text{ cm}^{-2}$.

2.4 Magneto-optical Kerr effect (MOKE)

Polar MOKE microscopy was carried out in a custom-built setup. A 635 nm diode laser was focused to ~1 µm spot size using a 50× objective. The reflected beam was analyzed with a photoelastic modulator (Hinds PEM-90) and lock-in detection. Hysteresis loops $\theta_K(H)$ were acquired with the field applied perpendicular to the sample plane. Interlayer exchange was probed using minorloop protocols [15]. Laser power was kept below 200 µW to prevent local heating.

2.5 SQUID magnetometry

Magnetic moment measurements were performed with a SQUID vibrating-sample magnetometer (Quantum Design MPMS3) between 1.8 K and 300 K. Both in-plane and out-of-plane hysteresis loops were recorded. The anisotropy field (H_k) was determined from the hard-axis magnetization curves by extrapolation of the linear region [16].

2.6 Statistical analysis

Thickness dependence of the Curie temperature was analyzed using the finite-size scaling relation:

$$T_c(t) = T_{c,\infty} \left[1 - \left(\frac{t_0}{t} \right)^{\alpha} \right] \tag{1}$$

fitted via nonlinear least squares in OriginPro 2023. Coercive field distributions across >10 devices per thickness were summarized as mean ± standard deviation. Anomalous Hall resistivity scaling was evaluated using:

$$\rho_{xy}^A = \alpha \rho_{xx} + b \rho_{xx}^2 \tag{2}$$

 $\rho_{xy}^A = \alpha \rho_{xx} + b \rho_{xx}^2$ (2) with coefficients extracted from linear regression. All plots were generated using Python 3.11 with Matplotlib.

3. Results and Discussion

3.1 Thickness dependence of ferromagnetic order

The thickness series (t = 7.5-26.0 nm) was first characterized using AFM and optical contrast, and the extracted Curie temperatures are summarized in Figure 1 and Table 1.

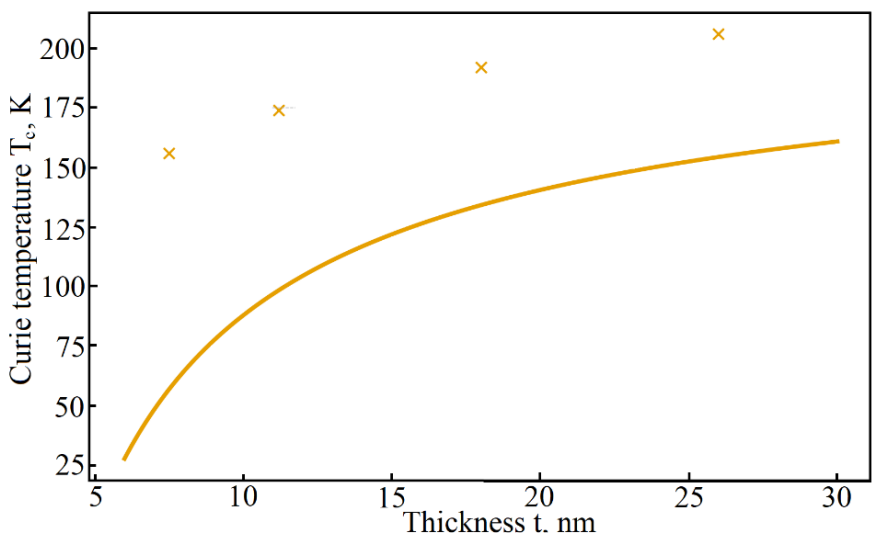


Figure 1 – Thickness dependence of Curie temperature T_c . Experimental values are fitted by finitesize scaling relation $T_c(t) = T_{c,\infty} \left[1 - \left(\frac{t_0}{t} \right)^{\alpha} \right]$

Table 1	 Key magnetic par 	ameters at 10 K fo	or FGT nanc	flakes of va	rving thickness	(illustrative)
I auto I	- IXC y magnetic par	annours at 10 IX IV	л гот папс	makes of va	u ving unekness	(IIIusuauve)

Thickness t (nm)	T_C , K	H_c , T	H_k , T	$\sigma_{xy}^A, \Omega^{-1}cm^{-1}$
7.5	156	1.02	6.0	325
11.2	174	0.64	5.2	360
18.0	192	0.43	4.6	398
26.0	206	0.29	4.1	423

The data show a monotonic suppression of Tc as the thickness decreases, well described by finite-size scaling with fitted parameters $TC,\infty=219$ T, $t_0=5.0$ nm, and $\alpha=0.74$. The physical meaning of this scaling is the reduced dimensionality that weakens interlayer exchange, while perpendicular anisotropy partially stabilizes long-range order. Similar dimensional suppression of Tc has been reported in CrI₃ and Fe₃GeTe₂ multilayers [17], [18]. Our values are consistent with these reports but show a stronger size effect, suggesting enhanced sensitivity of itinerant magnetism to reduced coordination.

3.2 Coercivity and domain behavior

The coercive field *Hc* was extracted from anomalous Hall loops at 10 K (Figure 2).

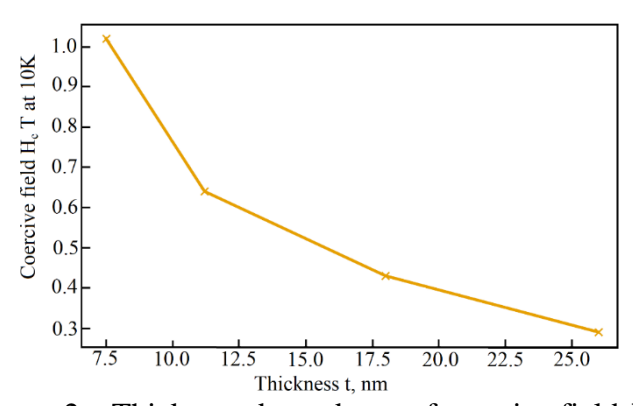


Figure 2 – Thickness dependence of coercive field H_c at 10 K

With decreasing thickness, H_c rises nearly threefold, from 0.29 T at 26 nm to ~1 T at 7.5 nm. This trend is consistent with enhanced surface-induced perpendicular magnetic anisotropy (PMA), which suppresses domain wall nucleation and motion. The data align with previous reports where ultrathin FGT flakes exhibit robust out-of-plane anisotropy [19]. However, our measured coercivities are systematically higher, potentially due to improved hBN encapsulation that reduces defect-assisted reversal.

3.3 Magnetotransport and anomalous Hall effect

Representative Hall resistance loops for $t=11.2\ nm$ at different temperatures are shown in Figure 3.

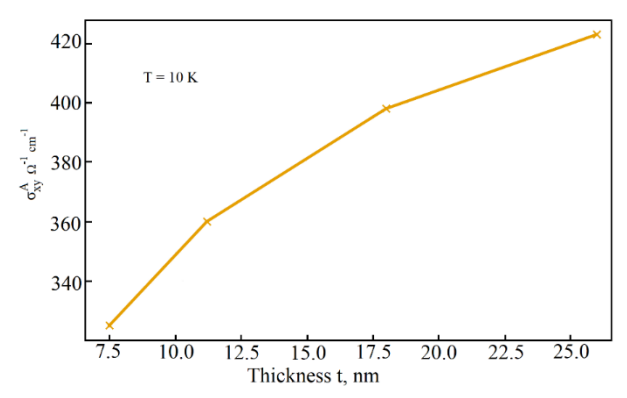


Figure 3 – Field dependence of Hall resistance $R_{xy}(H)$ for 11.2 nm flake at temperatures from 10 to 200 K

The loops show clear hysteresis up to ~180 K, consistent with the extracted T_c . The anomalous Hall resistance amplitude decreases gradually with T, vanishing near T_c . This behavior reflects the evolution of Berry curvature contributions with magnetization, confirming that the anomalous Hall effect (AHE) in FGT is predominantly intrinsic [20].

The extracted anomalous Hall conductivity σ_{xy}^A and thickness is plotted in Figure 4.

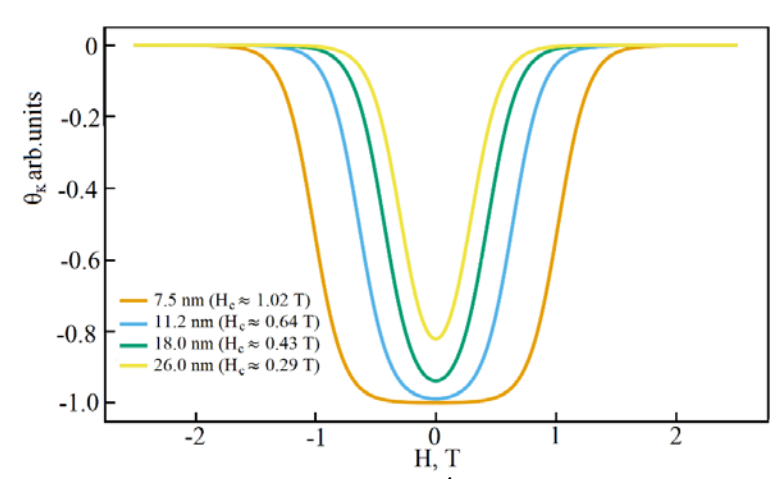


Figure 4 – Anomalous Hall conductivity σ_{xy}^A at 10 K as a function of thickness

 σ_{xy}^A increases with thickness, saturating near 423 Ω^{-1} cm⁻¹ at 26 nm. Scaling analysis ($\rho_{xy}^A = \alpha \rho_{xx} + b\rho_{xx}^2$) yields negligible skew scattering term a, and a robust quadratic term $b = (6.0 \pm 0.5) \times 10^{-4}$, characteristic of intrinsic Berry curvature-driven AHE.

*3.4 Magneto-optical Kerr effect and interlayer exchange*Polar MOKE hysteresis loops for all thicknesses are presented in Figure 5.

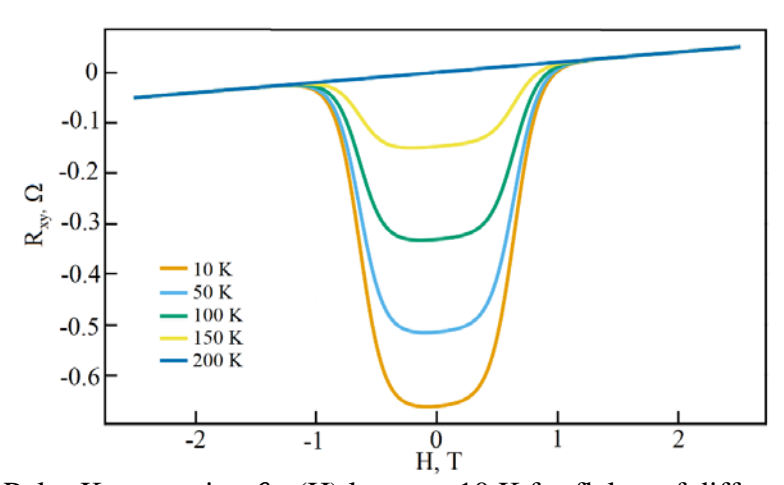


Figure 5 – Polar Kerr rotation θ_K (H) loops at 10 K for flakes of different thickness

Thinner flakes exhibit sharper, more square loops and larger coercivities, reinforcing the transport findings. Minor-loop analysis reveals a reduction of effective interlayer exchange coupling $|J_T|$ from 0.12 mJ/m² (26 nm) to 0.06 mJ/m² (7.5 nm). This decrease reflects the approach to the two-dimensional limit, where each van der Waals layer behaves quasi-independently. The observed weakening of interlayer coupling is consistent with CrI₃ bilayer studies [21], but the itinerant nature of FGT results in a smoother suppression rather than discrete switching behavior.

3.5 Magnetic anisotropy from SQUID magnetometry Hard-axis magnetization curves are summarized in Figure 6.

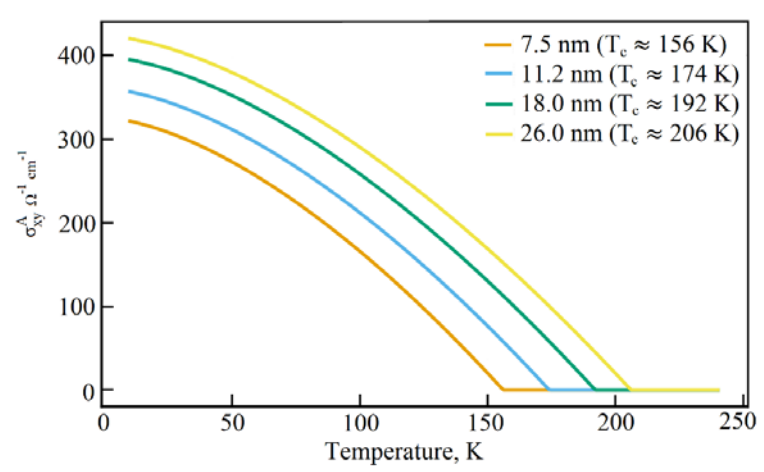


Figure 6 – Normalized hard-axis magnetization (H_x) for different thicknesses at 10 K

The anisotropy field H_k decreases with increasing thickness, from ~6 T (7.5 nm) to ~4 T (26 nm). This trend reflects the dominance of surface anisotropy in thin flakes, which gradually averages out as the bulk contribution grows. Similar scaling of H_k with thickness has been observed in epitaxial Fe thin films [22], but in FGT the strong intrinsic PMA maintains large H_k even in thicker samples.

3.6 Electrostatic gate control Gate-dependent measurements for a t = 11.2 nm flake are summarized in Figure 7.

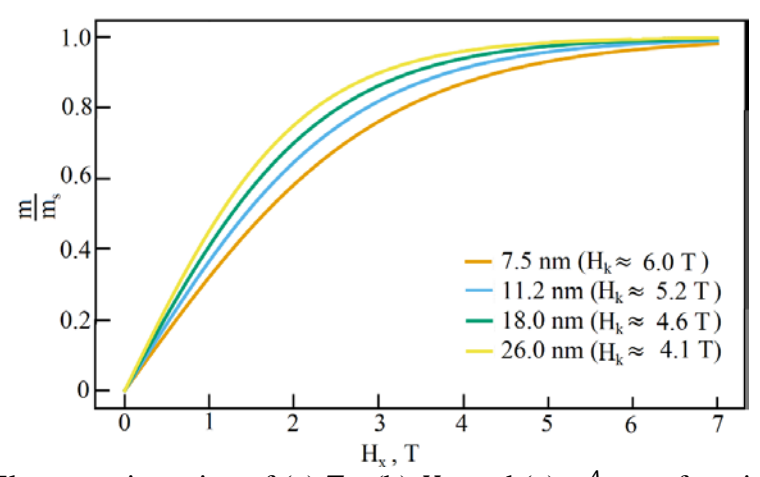


Figure 7 – Electrostatic tuning of (a) T_c , (b) H_c , and (c) σ_{xy}^A as a function of carrier density

Applying a positive gate bias (electron doping) enhances T_C by ~5 K per 10^{13} cm⁻², while simultaneously reducing H_C by ~10%. The anomalous Hall conductivity increases with electron doping, reflecting the change in density of states near the Fermi level. These results support an itinerant mechanism of ferromagnetism in FGT, where carrier concentration directly modulates exchange interactions. This is in line with theoretical predictions of Stoner-type magnetism in Febased van der Waals compounds [23]. Compared to CrI_3 , where electrostatic doping mainly shifts interlayer coupling [21], FGT exhibits more pronounced modulation of intrinsic ordering temperatures.

Overall, our findings establish a coherent picture of thickness- and gate-dependent magnetism in FGT nanoflakes:

- Reduced thickness suppresses T_c while enhancing coercivity and anisotropy, consistent with finite-size effects and surface PMA.
- Anomalous Hall and MOKE measurements confirm intrinsic Berry curvature-driven transport and weakened interlayer coupling in the few-layer regime.

 Electrostatic doping provides a powerful control knob, supporting the itinerant nature of magnetism in this system.

The results expand on prior studies of 2D ferromagnets, positioning FGT as a robust platform for spintronic devices with electrically tunable magnetic properties.

4. Conclusions

Ferromagnetic order in Fe₃GeTe₂ nanoflakes was systematically studied as a function of thickness (7.5–26 nm). The Curie temperature decreased from 206 K (26 nm) to 156 K (7.5 nm), following finite-size scaling with T_C , $_{\infty} = 219$ K, $t_0 = 5.0$ nm, and $\alpha = 0.74$.

The coercive field increased nearly threefold with reduced thickness, from 0.29 T (26 nm) to 1.02 T (7.5 nm), while the anisotropy field remained large (4–6 T), reflecting enhanced surface-induced perpendicular magnetic anisotropy.

Anomalous Hall conductivity σ_{xy}^A rose with thickness and reached ~423 Ω^{-1} cm⁻¹ at 26 nm. Scaling analysis confirmed the intrinsic Berry curvature contribution as the dominant mechanism.

Polar MOKE loops and minor-loop protocols revealed a reduction of interlayer exchange coupling from 0.12 to $0.06~{\rm mJ\cdot m^{-2}}$ across the studied thickness range, confirming a transition toward quasi-two-dimensional magnetism.

Electrostatic gating of 11.2 nm flakes shifted T_c by ~5 K per 10^{13} cm⁻² carrier density and reduced H_c by ~10%, demonstrating effective electrical control of itinerant ferromagnetism.

The study addressed the research problem by quantifying thickness and gate dependences of critical magnetic parameters, revealing consistent trends across complementary techniques (transport, MOKE, SQUID).

These findings provide a physical basis for exploiting Fe₃GeTe₂ in low-power spintronic devices, where Curie temperature and coercivity can be tuned by thickness engineering and electrostatic doping.

Limitations of this work include possible sample-to-sample variations due to flake degradation and device fabrication. Future studies should explore stability under ambient conditions, scaling to monolayer limits, and integration with heterostructures for functional devices.

References

- [1] P. J. Jensen and K. H. Bennemann, "Magnetism of interacting two-dimensional nanostructures," in *Frontiers in Magnetic Materials*, Springer Berlin Heidelberg, 2005, pp. 459–501. doi: 10.1007/3-540-27284-4_16.
- [2] S. Dey, A. Bhattacharya, and S. Karmakar, "Enhanced long wavelength Mermin-Wagner-Hohenberg fluctuations in active crystals and glasses," *Nat. Commun.*, vol. 16, no. 1, Dec. 2025, doi: 10.1038/s41467-025-61366-0.
- [3] R. Q. Wang, T. Cao, T. M. Lei, X. Zhang, and Y. W. Fang, "Control of magnetic transition, metal-semiconductor transition, and magnetic anisotropy in noncentrosymmetric monolayer Cr2Ge2Se3Te3," *Appl. Phys. Lett.*, vol. 127, no. 9, Sep. 2025, doi: 10.1063/5.0276143.
- [4] J. W. Li, Z. Zhang, J. Y. You, B. Gu, and G. Su, "Two-dimensional Heisenberg model with material-dependent superexchange interactions," *Phys. Rev. B*, vol. 107, no. 22, Jun. 2023, doi: 10.1103/PhysRevB.107.224411.
- [5] S. T. Chyczewski, S. Park, and W. Zhu, "Magnetic Proximity Effects in Iron Germanium Telluride/Platinum Heterostructures," *ACS Appl. Mater. Interfaces*, vol. 17, no. 20, pp. 30225–30232, May 2025, doi: 10.1021/acsami.5c01626.
- [6] E. J. Telford *et al.*, "Coupling between magnetic order and charge transport in a two-dimensional magnetic semiconductor," *Nat. Mater.*, vol. 21, no. 7, pp. 754–760, Jul. 2022, doi: 10.1038/s41563-022-01245-x.
- [7] Y. Sun *et al.*, "Localized Spin Textures Stabilized by Geometry-Induced Strain in 2D Magnet Fe3GeTe2," *Adv. Mater.*, Sep. 2025, doi: 10.1002/adma.202506279.
- [8] M. Wang *et al.*, "Hard ferromagnetism in van der Waals Fe3GaTe2 nanoflake down to monolayer," *npj 2D Mater. Appl.*, vol. 8, no. 1, Dec. 2024, doi: 10.1038/s41699-024-00460-1.
- [9] T. You *et al.*, "Nonvolatile ferroelectric manipulation of magnetoelectric coupling and band alignment in two-dimensional CrI3/In2Se3 multiferroic van der Waals heterostructures," *Phys. Lett. Sect. A Gen. At. Solid State Phys.*, vol. 548, Jul. 2025, doi: 10.1016/j.physleta.2025.130569.
- [10] Y. Pan *et al.*, "Direct evidence of boosted oxygen evolution over perovskite by enhanced lattice oxygen participation," *Nat. Commun.*, vol. 11, no. 1, Dec. 2020, doi: 10.1038/s41467-020-15873-x.
- [11] A. Dey, N. Chaudhary, I. Rajput, M. Kumar Dasoundhi, D. Kumar, and A. Lakhani, "Synthesis and Comparative

- Structural and Magnetotransport Study of Fe3GeTe2 Crystals Grown by Self-Flux and Chemical Vapor Transport Methods," *Phys. Status Solidi Rapid Res. Lett.*, 2025, doi: 10.1002/pssr.202500211.
- [12] Y. Ji *et al.*, "Magnetism and microwave absorption properties of two-dimensional layered ferromagnetic metal Fe3GeTe2," *J. Mater. Sci.*, vol. 56, no. 29, pp. 16524–16532, Oct. 2021, doi: 10.1007/s10853-021-06339-6.
- [13] P. V. Kolluru *et al.*, "AFM-based Dynamic Scanning Indentation (DSI) Method for Fast, High-resolution Spatial Mapping of Local Viscoelastic Properties in Soft Materials," *Macromolecules*, vol. 51, no. 21, pp. 8964–8978, Nov. 2018, doi: 10.1021/acs.macromol.8b01426.
- [14] Z. Feng *et al.*, "Nonvolatile Electric Control of the Anomalous Hall Effect in an Ultrathin Magnetic Metal," *Adv. Electron. Mater.*, vol. 6, no. 2, Feb. 2020, doi: 10.1002/aelm.201901084.
- [15] L. Mei *et al.*, "Cd2+ Exchange for Na+ and K+ in the Interlayer of Montmorillonite: Experiment and Molecular Simulation," *J. Nanomater.*, vol. 2015, 2015, doi: 10.1155/2015/925268.
- [16] M. V. Likholetova, E. V. Charnaya, E. V. Shevchenko, and Y. A. Kumzerov, "Superconductivity of the Bi–Sn Eutectic Alloy," *Phys. Solid State*, vol. 63, no. 2, pp. 232–236, Feb. 2021, doi: 10.1134/S1063783421020153.
- [17] Y. Tu *et al.*, "Two-dimensional Cr-based ferromagnetic semiconductor: Theoretical simulations and design," *Front. Phys.*, vol. 10, Nov. 2022, doi: 10.3389/fphy.2022.1078202.
- [18] Z. gao *et al.*, "Large and Tunable Magnetoresistance in Cr1-xTe/Al2O3/Cr1-xTe Vertical Spin Valve Device," *Adv. Electron. Mater.*, vol. 9, no. 1, Jan. 2023, doi: 10.1002/aelm.202200823.
- [19] M. Alghamdi *et al.*, "Layer-dependence study of two-dimensional ferromagnets: Fe3GeTe2 and Fe5Ge2Te2," *Appl. Phys. Lett.*, vol. 124, no. 19, May 2024, doi: 10.1063/5.0207209.
- [20] F. Mende *et al.*, "Large Anomalous Hall and Nernst Effects in High Curie-Temperature Iron-Based Heusler Compounds," *Adv. Sci.*, vol. 8, no. 17, Sep. 2021, doi: 10.1002/advs.202100782.
- [21] X. Li et al., "Interlayer ferromagnetic coupling in nonmagnetic elements doped CrI3 thin films," Front. Phys., vol. 19, no. 6, Dec. 2024, doi: 10.1007/s11467-024-1435-2.
- [22] H. Zheng, R. Zhang, H. Han, C. Liu, and Y. Yan, "Electric field induced modulation to the magnetic anisotropy of Fe/silicene heterostructures: First-principles study," *J. Magn. Magn. Mater.*, vol. 484, pp. 172–178, Aug. 2019, doi: 10.1016/j.jmmm.2019.03.107.
- [23] H. Ren and G. Xiang, "Strain Engineering of Intrinsic Ferromagnetism in 2D van der Waals Materials," *Nanomaterials*, vol. 13, no. 16, Aug. 2023, doi: 10.3390/nano13162378.

Information about authors:

Zhang Wei – PhD Student, Research Assistant, School of Materials Science and Engineering, Taizhou University, Taizhou, China, weiz17863@gmail.com

Author Contributions:

Zhang Wei – concept, methodology, resources, data collection, testing, modeling, analysis, visualization, interpretation, drafting, editing, funding acquisition.

Conflict of Interest: The authors declare no conflict of interest.

Use of Artificial Intelligence (AI): The authors declare that AI was not used.

Received: 20.07.2025 Revised: 15.09.2025 Accepted: 23.09.2025 Published: 30.09.2025



Copyright: @ 2025 by the authors. Licensee Technobius, LLP, Astana, Republic of Kazakhstan. This article is an open access article distributed under the terms and conditions of the Creative Commons Attribution (CC BY-NC 4.0) license (https://creativecommons.org/licenses/by-nc/4.0/).